

# Effects of mixing on post-discharge modeling of ElectricOIL experiments

Andrew D. Palla<sup>a</sup>, David L. Carroll<sup>a\*</sup>, Joseph T. Verdeyen<sup>a</sup>, and Wayne C. Solomon<sup>b</sup>

<sup>a</sup>CU Aerospace, 60 Hazelwood Drive, Champaign, IL 61820;

<sup>b</sup>Dept. Aero. Eng., Univ. of Ill. at Urbana-Champaign, 104 S. Wright St., Urbana, IL 61801

## ABSTRACT

In an electric discharge Oxygen-Iodine laser (ElectricOIL), the desired  $O_2(a^1\Delta)$  is produced using a low-to-medium pressure electric discharge. The discharge production of atomic oxygen, ozone, and other excited species adds higher levels of complexity to the post-discharge kinetics which are not encountered in a classic purely chemical  $O_2(a^1\Delta)$  generation system. Mixing effects are also present. In this paper we present post-discharge modeling results obtained using a modified version of the Blaze-II gas laser code. A 28 specie, 105 reaction chemical kinetic reaction set for the post-discharge kinetics is presented. Calculations were performed to ascertain the impact of a two stream mixing mechanism on the numerical model and to study gain as a function of reactant mass flow rates. The calculations were compared with experimental data. Agreement with experimental data was improved with the addition of new kinetics and the mixing mechanism.

**Keywords:** Mixing effects, post-discharge modeling, ElectricOIL, DOIL, electric discharge oxygen-iodine laser

## 1. INTRODUCTION

Oxygen-iodine laser systems<sup>1</sup> operate on the  $I(^2P_{1/2}) \rightarrow I(^2P_{3/2})$  [hereafter denoted  $I^*$  and  $I$ , respectively] electronic transition of the iodine atom at 1315 nm. The population inversion is produced by the near resonant energy transfer between the metastable excited singlet oxygen molecule,  $O_2(a^1\Delta)$  [also denoted  $O_2(a)$  hereafter], and the atomic iodine ground state. There are many system issues having to do with weight, safety and operational logistics in the production of the  $O_2(a)$  by chemical means which have motivated investigations into methods to produce significant amounts of  $O_2(a)$  using flowing electric discharges. Several investigations have been conducted into the possibility of a continuous flow hybrid electrically powered oxygen-iodine laser with electric discharges to produce the  $O_2(a)$ .<sup>2-9</sup> These studies have shown that flowing oxygen containing mixtures, typically diluted with a rare gas, through electric discharges can produce useful quantities of  $O_2(a)$ . Recent experimental studies using electric discharges have demonstrated  $O_2(a)$  yields greater than 15% using electric discharges,<sup>4,5,7-9</sup> gain,<sup>10-12</sup> and cw laser power.<sup>13-14</sup> Several modeling studies<sup>2,5,6,15</sup> have also been performed for ElectricOIL and similar systems.

Since ElectricOIL development is impacted by an imperfect understanding of post-discharge physics, the Blaze-II chemical laser model<sup>16</sup> was improved to allow more extensive studies of ElectricOIL post-discharge kinetics and laser performance. In this paper, we present the results of a study with an updated and more comprehensive reaction set than previously utilized.<sup>2</sup> The impact of a two stream mixing mechanism, defined in terms of diffusion coefficients and a scheduled mixing approach, is examined. Simulations are compared with experimental data. Also presented is a study of laser gain as a function of reactant mass flow rates.

## 2. THE BLAZE-II GAS LASER MODEL

The Blaze-II code<sup>16</sup> was originally written to be as generic a gas laser model as possible. Blaze-II can treat arbitrary combinations of chemical species characterized by as many as 500 reactions and 40 species. Blaze-II, which contains one-dimensional fluid dynamic equations whose mixing terms are derived from the two-dimensional (2-D) equations that describe the mixing flow field in a gas laser cavity, can be used for axisymmetric and 2-D flows. Lasing may occur on a single atomic transition or on as many as 10 vibrational bands of a diatomic species. Blaze-II is capable of performing premixed and mixing calculations. The gain  $g$  of an iodine laser is given by<sup>17-19</sup>

\*carroll@cuaerospace.com; phone 217-333-8274; cuaerospace.com

$$g = \frac{7}{12} \left( \frac{A_{21} \lambda^2}{8\pi} \right) \phi(\nu) \left( N_{I^*} - \frac{1}{2} N_I \right) \quad (1)$$

where  $\lambda = 1315$  nm,  $A_{21} = 5.0$  s<sup>-1</sup>,  $N_{I^*}$  and  $N_I$  are the number densities of excited atomic iodine,  $I^*$ , and ground state atomic iodine,  $I$ , and the Voigt lineshape function  $\phi(\nu_0)$  at line center is given by

$$\phi(\nu_0) = \frac{2}{\Delta\nu_D} \left( \frac{\ell n 2}{\pi} \right)^{1/2} [1 - \text{erf}(y)] \exp(y^2) \quad (2)$$

where

$$\Delta\nu_D = \frac{2}{\lambda} \sqrt{\frac{2RT \ell n 2}{W}} = 1.4492 \times 10^7 \sqrt{T} \quad (3)$$

$$y = \frac{\Delta\nu_L}{\Delta\nu_D} \sqrt{\ell n 2} \quad (4)$$

$$\Delta\nu_L = P \sqrt{\frac{T_{ref}}{T}} \sum_i \alpha_i x_i \quad (5)$$

$R$  is the universal gas constant (8.314 J/mole-°K),  $W$  is the molecular weight of Iodine (126.9 gm/mole),  $T$  is the temperature in °K,  $T_{ref}$  is a reference temperature taken to be 295 °K,  $P$  is the pressure in Torr,  $x_i$  is the mole fraction of species  $i$ , and the pressure broadening coefficients  $\alpha_i$  in MHz/Torr (referenced to 295°K) are 2.4, 5.5, 5.0, 3.2, 5.5, and 2.6 for I, I<sub>2</sub>, O<sub>2</sub>, He, N<sub>2</sub>, and Ar respectively.<sup>18,36,39</sup>

The Blaze-II code was originally written to model a gas laser in which reactants are injected at a single point. To permit the injection of reactants at an arbitrary number of points at arbitrary locations, the Blaze-II code was modified. This modification allows the code to better model the current ElectricOIL system in which reactants are injected at as many as four positions. Automation was added to the code that allows large parametric studies to be input, completed, and reduced quickly. The optimization of the code was substantially improved in order to further reduce run times. Blaze-II COIL runs using a 33 reaction, 12 specie set had previously required ~30 CPU seconds on an IBM RS/6000 machine,<sup>20</sup> whereas current Blaze-II ElectricOIL runs using a 105 reaction, 28 specie set now require ~2 CPU seconds on an Intel Pentium 4 machine, and only ~1 CPU second on a Macintosh G5. Code was added to automatically reduce calculation results from multiple cases in large studies. The improvements in optimization and automation have made it possible to complete and quickly analyze large parametric studies on the order of tens of thousands of cases.

The Blaze-II calculations presented in this paper are based on a four section/injection-point ElectricOIL format<sup>11</sup>, with the following sections (i) discharge output flow, (ii) NO<sub>2</sub> injection, (iii) I<sub>2</sub> injection, and (iv) tertiary diluent (Ar/N<sub>2</sub>) injection, as shown in Fig. 1. The flow tube is approximately 4.9 cm in diameter and exhausts through a Mach 2 nozzle. Simulations begin at the exit of the discharge (which is treated as the first reactant section, X=0 cm), NO<sub>2</sub> is injected at X=53 cm, an I<sub>2</sub>/He mixture is injected at X=81.9 cm, Ar or N<sub>2</sub> is injected at X=117.5 cm, and the nozzle throat is at X=141.63 cm. The subsonic diagnostic port, hereafter referred to as the diagnostic port, is at X=101.9 cm.

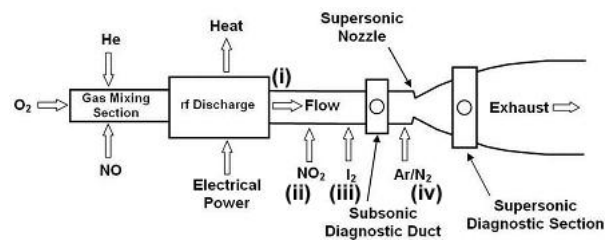


Figure 1: Schematic of ElectricOIL apparatus that was modeled.

### 3. BLAZE-II KINETIC SIMULATIONS

The accuracy of Blaze-II calculations is critically dependent on the accuracy of the input chemical kinetic reaction set. Several  $I^*$ ,  $O_2(a^1\Delta)$ ,  $O_2(b^1\Sigma)$  [also denoted  $O_2(b)$  hereafter], NO, and NO<sub>2</sub> dependent reactions that were not included in previous Blaze-II ElectricOIL modeling<sup>2</sup> may affect the accuracy of the model. As such, the chemical kinetic reaction set was expanded to include 28 species and 105 reactions, Table 1. Note that a number of temperature dependent reactions have been included because the temperature range in the post-discharge laser system can be as large as 600 K at the exit of the discharge to near 100 K in the supersonic laser cavity.

Table 1: Blaze-II ElectricOIL 105 reaction, 28 specie set and reaction rates. Reaction rates for three-body reactions have units  $\text{cm}^6/\text{molecule}^2\text{-s}$ . Certain specified quenching reactions have been assumed from other known reactions.

$k$	Reaction						Rate, $\text{cm}^3/\text{molecule-s}$	Ref.	
1	$\text{O}_2(^1\Delta)$	+	$\text{O}_2(^1\Delta)$	$\rightarrow$	$\text{O}_2(^1\Sigma)$	+	$\text{O}_2$	$9.8\text{e-}28 \times \text{T}^{3.8} \times \exp(700/\text{T})$	Perram [26]
2	$\text{O}_2(^1\Delta)$	+	$\text{O}_2(^1\Delta)$	$\rightarrow$	$\text{O}_2$	+	$\text{O}_2$	1.7e-17	Perram [26]
3	$\text{O}_2$	+	$\text{O}_2(^1\Sigma)$	$\rightarrow$	$\text{O}_2(^1\Delta)$	+	$\text{O}_2$	3.7e-17	Han [27]
4	$\text{O}_2(^1\Sigma)$	+	$\text{H}_2\text{O}$	$\rightarrow$	$\text{O}_2(^1\Delta)$	+	$\text{H}_2\text{O}$	6.7e-12	Perram [26]
5	$\text{O}_2(^1\Sigma)$	+	$\text{Cl}_2$	$\rightarrow$	$\text{O}_2(^1\Delta)$	+	$\text{Cl}_2$	2.0e-15	Perram [26]
6	$\text{O}_2(^1\Sigma)$	+	$\text{He}$	$\rightarrow$	$\text{O}_2(^1\Delta)$	+	$\text{He}$	1.0e-17	Perram [26]
7	$\text{O}_2(^1\Sigma)$	+	$\text{Ar}$	$\rightarrow$	$\text{O}_2(^1\Delta)$	+	$\text{Ar}$	1.0e-17	From #6
8	$\text{O}_2(^1\Sigma)$	+	$\text{Xe}$	$\rightarrow$	$\text{O}_2(^1\Delta)$	+	$\text{Xe}$	1.0e-17	From #6
9	$\text{O}_2$	+	$\text{O}_2(^1\Delta)$	$\rightarrow$	$\text{O}_2$	+	$\text{O}_2$	8.2e-19	Han [27]
10	$\text{O}_2(^1\Delta)$	+	$\text{H}_2\text{O}$	$\rightarrow$	$\text{O}_2$	+	$\text{H}_2\text{O}$	4.0e-18	Perram [26]
11	$\text{O}_2(^1\Delta)$	+	$\text{Cl}_2$	$\rightarrow$	$\text{O}_2$	+	$\text{Cl}_2$	6.0e-18	Perram [26]
12	$\text{O}_2(^1\Delta)$	+	$\text{He}$	$\rightarrow$	$\text{O}_2$	+	$\text{He}$	8.0e-21	Perram [26]
13	$\text{O}_2(^1\Delta)$	+	$\text{Ar}$	$\rightarrow$	$\text{O}_2$	+	$\text{Ar}$	8.0e-21	From #12
14	$\text{O}_2(^1\Delta)$	+	$\text{Xe}$	$\rightarrow$	$\text{O}_2$	+	$\text{Xe}$	8.0e-21	From #12
15	$\text{O}_2(^1\Delta)$	+	$\text{N}_2$	$\rightarrow$	$\text{O}_2$	+	$\text{N}_2$	1.4e-19	Atkinson [24]
16	$\text{O}_2(^1\Sigma)$	+	$\text{N}_2$	$\rightarrow$	$\text{O}_2$	+	$\text{N}_2$	2.0e-16	Atkinson [24]
17	$\text{O}_2(^1\Sigma)$	+	$\text{N}_2$	$\rightarrow$	$\text{O}_2(^1\Delta)$	+	$\text{N}_2$	1.8e-15	Atkinson [24]
18	$\text{O}_2(^1\Sigma)$	+	$\text{I}_2$	$\rightarrow$	$\text{O}_2$	+	$2\text{I}$	2.8e-11	Heaven [35]
19	$\text{O}_2(^1\Sigma)$	+	$\text{I}_2$	$\rightarrow$	$\text{O}_2(^1\Delta)$	+	$\text{I}_2$	2.3e-11	Han [27]
20	$\text{O}_2(^1\Sigma)$	+	$\text{I}_2$	$\rightarrow$	$\text{O}_2$	+	$\text{I}_2$	6.0e-12	Heaven [35]
21	$\text{O}_2(^1\Delta)$	+	$\text{I}_2$	$\rightarrow$	$\text{O}_2$	+	$\text{I}_2^*$	7.0e-15	Perram [26]
22	$\text{O}_2(^1\Delta)$	+	$\text{I}_2$	$\rightarrow$	$\text{O}_2$	+	$\text{I}_2^*$	5.0e-16	Han [27]
23	$\text{I}^*$	+	$\text{I}_2$	$\rightarrow$	$\text{I}$	+	$\text{I}_2^*$	$1.4\text{e-}13 \times \exp(1600/\text{T})$	Perram [26]
24	$\text{O}_2(^1\Delta)$	+	$\text{I}_2^*$	$\rightarrow$	$\text{O}_2$	+	$2\text{I}$	3.0e-10	Perram [26]
25	$\text{I}_2^*$	+	$\text{O}_2$	$\rightarrow$	$\text{I}_2$	+	$\text{O}_2$	4.9e-12	Heaven [28]
26	$\text{I}_2^*$	+	$\text{H}_2\text{O}$	$\rightarrow$	$\text{I}_2$	+	$\text{H}_2\text{O}$	1.7e-11	Heaven [28]
27	$\text{I}_2^*$	+	$\text{He}$	$\rightarrow$	$\text{I}_2$	+	$\text{He}$	9.8e-12	Heaven [28]
28	$\text{I}_2^*$	+	$\text{Ar}$	$\rightarrow$	$\text{I}_2$	+	$\text{Ar}$	4.0e-12	Perram [26]
29	$\text{I}_2^*$	+	$\text{Xe}$	$\rightarrow$	$\text{I}_2$	+	$\text{Xe}$	4.0e-12	From #28
30	$\text{I}_2^*$	+	$\text{Cl}_2$	$\rightarrow$	$\text{I}_2$	+	$\text{Cl}_2$	6.3e-12	Heaven [28]
31	$\text{I}_2^*$	+	$\text{N}_2$	$\rightarrow$	$\text{I}_2$	+	$\text{N}_2$	8.2e-12	Heaven [29]
32	$\text{I}^*$	+	$\text{O}_2(^1\Delta)$	$\rightarrow$	$\text{I}^*$	+	$\text{O}_2$	$2.3\text{e-}8 \times \text{T}^{-1}$	Perram [26]
33	$\text{I}^*$	+	$\text{O}_2$	$\rightarrow$	$\text{I}$	+	$\text{O}_2(^1\Delta)$	$3.1\text{e-}8 \times \text{T}^{-1} \times \exp(-403/\text{T})$	Perram [26]
34	$\text{I}^*$	+	$\text{O}_2(^1\Delta)$	$\rightarrow$	$\text{I}$	+	$\text{O}_2$	1.0e-15	Perram [26]
35	$\text{I}^*$	+	$\text{O}_2$	$\rightarrow$	$\text{I}$	+	$\text{O}_2$	3.5e-16	Perram [26]
36	$\text{I}^*$	+	$\text{O}_2(^1\Delta)$	$\rightarrow$	$\text{I}$	+	$\text{O}_2(^1\Sigma)$	$4.0\text{e-}24 \times \text{T}^{3.8} \times \exp(700/\text{T})$	Perram [26]
37	$\text{I}^*$	+	$\text{O}_2(^1\Delta)$	$\rightarrow$	$\text{I}$	+	$\text{O}_2(^1\Delta)$	1.1e-13	Perram [26]
38	$\text{I}^*$	+	$\text{I}$	$\rightarrow$	$\text{I}$	+	$\text{I}$	1.7e-13	Perram [26]
39	$\text{I}^*$	+	$\text{H}_2\text{O}$	$\rightarrow$	$\text{I}$	+	$\text{H}_2\text{O}$	2.1e-12	Perram [26]
40	$\text{I}^*$	+	$\text{He}$	$\rightarrow$	$\text{I}$	+	$\text{He}$	5.0e-18	Perram [26]
41	$\text{I}^*$	+	$\text{N}_2$	$\rightarrow$	$\text{I}$	+	$\text{N}_2$	6.5e-17	Deakin [30]
42	$\text{I}^*$	+	$\text{Ar}$	$\rightarrow$	$\text{I}$	+	$\text{Ar}$	5.0e-18	From #40
43	$\text{I}^*$	+	$\text{Xe}$	$\rightarrow$	$\text{I}$	+	$\text{Xe}$	5.0e-18	From #40
44	$\text{I}^*$	+	$\text{Cl}_2$	$\rightarrow$	$\text{ICl}$	+	$\text{Cl}$	5.5e-15	Perram [26]
45	$\text{I}^*$	+	$\text{Cl}_2$	$\rightarrow$	$\text{I}$	+	$\text{Cl}_2$	8.0e-15	Perram [26]
46	$\text{I}^*$	+	$\text{ICl}$	$\rightarrow$	$\text{I}_2$	+	$\text{Cl}$	1.5e-11	Perram [26]
47	$\text{I}_2$	+	$\text{Cl}$	$\rightarrow$	$\text{I}$	+	$\text{ICl}$	2.0e-10	Perram [26]
48	$\text{ICl}$	+	$\text{Cl}$	$\rightarrow$	$\text{I}$	+	$\text{Cl}_2$	8.0e-12	Perram [26]
49	$\text{I}_2$	+	$2\text{I}$	$\rightarrow$	$\text{I}_2$	+	$\text{I}_2$	3.6e-30	Perram [26]
50	$\text{N}_2$	+	$2\text{I}$	$\rightarrow$	$\text{N}_2$	+	$\text{I}_2$	4.2e-33	Busch [31]
51	$\text{O}_2$	+	$2\text{I}$	$\rightarrow$	$\text{O}_2(^1\Delta)$	+	$\text{I}_2$	3.7e-33	Han [27]
52	$\text{O}_2$	+	$2\text{I}$	$\rightarrow$	$\text{O}_2$	+	$\text{I}_2$	3.3e-32	Han [27]
53	$\text{He}$	+	$2\text{I}$	$\rightarrow$	$\text{He}$	+	$\text{I}_2$	3.8e-33	Busch [31]

54	I <sub>2</sub>	+	I* + I	→	I <sub>2</sub> (B)	+	I <sub>2</sub>	3.6e-30	Perram [26]
55			I <sub>2</sub> (B)	→	I	+	I	1.0e6	Perram [26]
56	2O	+	He	→	O <sub>2</sub>	+	He	4.5e-34×exp(630/T)	Herron [32]
57	2O	+	O <sub>2</sub>	→	O <sub>2</sub>	+	O <sub>2</sub>	4.5e-34×exp(630/T)	Herron [32]
58	2O	+	O <sub>2</sub> ( <sup>1</sup> Δ)	→	O <sub>2</sub>	+	O <sub>2</sub> ( <sup>1</sup> Δ)	4.5e-34×exp(630/T)	Herron [32]
59	2O	+	Ar	→	O <sub>2</sub>	+	Ar	4.5e-34×exp(630/T)	From #56-58
60	2O	+	Xe	→	O <sub>2</sub>	+	Xe	4.5e-34×exp(630/T)	From #56-58
61	3O			→	O <sub>2</sub>	+	O	4.5e-34×exp(630/T)	Herron [32]
62	O	+	O <sub>2</sub> + He	→	O <sub>3</sub>	+	He	5.1e-27×T <sup>-2.8</sup>	Atkinson [24]
63	O	+	2O <sub>2</sub>	→	O <sub>3</sub>	+	O <sub>2</sub>	5.1e-27×T <sup>-2.8</sup>	Atkinson [24]
64	O	+	O <sub>2</sub> + O <sub>2</sub> ( <sup>1</sup> Δ)	→	O <sub>3</sub>	+	O <sub>2</sub> ( <sup>1</sup> Δ)	5.1e-27×T <sup>-2.8</sup>	Atkinson [24]
65	O	+	O <sub>2</sub> + Ar	→	O <sub>3</sub>	+	Ar	5.1e-27×T <sup>-2.8</sup>	From #62
66	O	+	O <sub>2</sub> + Xe	→	O <sub>3</sub>	+	Xe	5.1e-27×T <sup>-2.8</sup>	From #62
67	2O	+	O <sub>2</sub>	→	O <sub>3</sub>	+	O	5.1e-27×T <sup>-2.8</sup>	Atkinson [24]
68	O <sub>2</sub> ( <sup>1</sup> Δ)	+	O	→	O <sub>2</sub>	+	O	2.0e-16	Herron [32]
69	O <sub>2</sub> ( <sup>1</sup> Σ)	+	O	→	O <sub>2</sub> ( <sup>1</sup> Δ)	+	O	7.2e-14	Atkinson [24]
70	O <sub>2</sub> ( <sup>1</sup> Σ)	+	O	→	O <sub>2</sub>	+	O	8.0e-15	Atkinson [24]
71	O <sub>2</sub> ( <sup>1</sup> Σ)	+	O <sub>3</sub>	→	2O <sub>2</sub>	+	O	1.5e-11	Atkinson [24]
72	O <sub>2</sub> ( <sup>1</sup> Σ)	+	O <sub>3</sub>	→	O <sub>2</sub> ( <sup>1</sup> Δ)	+	O <sub>3</sub>	3.3e-12	Atkinson [24]
73	O <sub>2</sub> ( <sup>1</sup> Σ)	+	O <sub>3</sub>	→	O <sub>2</sub>	+	O <sub>3</sub>	3.3e-12	Atkinson [24]
74	O <sub>2</sub> (v)	+	O <sub>2</sub>	→	O <sub>2</sub>	+	O <sub>2</sub>	4.0e-14	Atkinson [24]
75	O <sub>2</sub> (v)	+	He	→	O <sub>2</sub>	+	He	1.3e-13	Atkinson [24]
76	O	+	O <sub>3</sub>	→	O <sub>2</sub>	+	O <sub>2</sub>	8.0e-12×exp(-2060/T)	Atkinson [24]
77	O <sub>2</sub> ( <sup>1</sup> Δ)	+	O <sub>3</sub>	→	2O <sub>2</sub>	+	O	5.2e-11×exp(-2840/T)	Atkinson [24]
78	I <sub>2</sub>	+	O	→	IO	+	I	1.4e-10	Atkinson [24]
79	IO	+	O	→	O <sub>2</sub>	+	I	1.4e-10	Han [27]
80	IO	+	O	→	O <sub>2</sub> ( <sup>1</sup> Δ)	+	I	1.5e-11	Han [27]
81	IO	+	IO	→	O <sub>2</sub>	+	2I	8.2e-11	Han [27]
82	I	+	O <sub>3</sub>	→	IO	+	O <sub>2</sub>	2.0e-11×exp(-890/T)	Atkinson [24]
83	I*	+	O	→	I	+	O	8e-12	Heaven [35]
84	NO <sub>2</sub>	+	O	→	O <sub>2</sub>	+	NO	6.5e-12×exp(120/T)	Atkinson [24]
85	NO <sub>2</sub>	+	O	→	O <sub>2</sub> ( <sup>1</sup> Δ)	+	NO	0.0	Atkinson [24]
86	NO <sub>2</sub>	+	O	→	O <sub>2</sub> ( <sup>1</sup> Σ)	+	NO	0.0	Atkinson [24]
87	O	+	NO	→	NO <sub>2</sub> *			2.5e-17	Kaufman [33]
88	NO <sub>2</sub> *			→	NO <sub>2</sub>			5.54e-20	Kaufman [33]
89	O( <sup>1</sup> D)	+	O <sub>2</sub>	→	O	+	O <sub>2</sub> ( <sup>1</sup> Σ)	2.6e-11×exp(67/T)	Atkinson [24]
90	O( <sup>1</sup> D)	+	O <sub>2</sub>	→	O	+	O <sub>2</sub> ( <sup>1</sup> Δ)	1.6e-12×exp(67/T)	Atkinson [24]
91	O( <sup>1</sup> D)	+	O <sub>2</sub>	→	O	+	O <sub>2</sub>	4.8e-12×exp(67/T)	Atkinson [24]
92	O( <sup>1</sup> D)	+	O <sub>3</sub>	→	2O	+	O <sub>2</sub>	1.2e-10	Atkinson [24]
93	O( <sup>1</sup> D)	+	O <sub>3</sub>	→	O <sub>2</sub>	+	O <sub>2</sub>	1.2e-10	Atkinson [24]
94	O <sub>2</sub> ( <sup>1</sup> Σ)	+	CO <sub>2</sub>	→	O <sub>2</sub> ( <sup>1</sup> Δ)	+	CO <sub>2</sub>	4.1e-13	Atkinson [24]
95	I*	+	NO	→	I	+	NO	1.2e-13	Heaven [21]
96	I*	+	NO <sub>2</sub>	→	I	+	NO <sub>2</sub>	8.5e-14	Han [22]
97	O <sub>2</sub> ( <sup>1</sup> Σ)	+	NO <sub>2</sub>	→	O <sub>2</sub> ( <sup>1</sup> Δ)	+	NO <sub>2</sub>	4.1e-13	Atkinson [24]
98	O <sub>2</sub> ( <sup>1</sup> Δ)	+	O <sub>2</sub> + O	→	2O <sub>2</sub>	+	O	1.0e-32	Vasiljeva [23]
99	O	+	NO + O <sub>2</sub>	→	NO <sub>2</sub>	+	O <sub>2</sub>	4.68e-28×T <sup>-1.5</sup>	Atkinson [24]
100	O	+	NO + He	→	He	+	NO <sub>2</sub>	2.08e-28×T <sup>-1.41</sup>	Atkinson [24]
101	O <sub>2</sub> ( <sup>1</sup> Σ)	+	NO	→	O <sub>2</sub> ( <sup>1</sup> Δ)	+	NO	6.0e-14	Atkinson [24]
102	O <sub>2</sub>	+	2NO	→	2NO <sub>2</sub>			3.3e-39×exp(530/T)	Atkinson [24]
103	NO <sub>2</sub>	+	O <sub>2</sub>	→	NO	+	O <sub>3</sub>	1.8e-12×exp(1370/T)	Atkinson [24]
104	O <sub>2</sub> ( <sup>1</sup> Δ)	+	CO <sub>2</sub>	→	O <sub>2</sub>	+	CO <sub>2</sub>	2.0e-20	Atkinson [24]
105	O <sub>2</sub> ( <sup>1</sup> Δ)	+	NO <sub>2</sub>	→	O <sub>2</sub>	+	NO <sub>2</sub>	2.0e-20	From #104

Data showed that although atomic oxygen produced by the rf discharge plays a positive role in the chemistry of the laser by dissociating  $I_2$ , it also plays a negative role by quenching  $I^*$ .<sup>11</sup> In order to eliminate the negative effects of atomic oxygen,  $NO_2$  was used to scavenge some of the O atoms upstream of the  $I_2$  injection point, as shown in Fig. 1.<sup>11</sup> As such, a numerical study was performed to determine if we could model the experimental  $O_2(a)$ ,  $I^*$ , and  $O_2(b)$  concentrations, and gain data as a function of rf discharge power and  $NO_2$  flow rate with the reaction set given in Table 1. The calculations used molar flow rates of  $O_2:He:I_2 = 4:16:0.008$  mmol/s and were performed for rf discharge powers from 4 to 800 Watts (in 4 Watt increments), for each  $NO_2$  flow rate of 0.0, 0.1, 0.2, 0.5, and 1.0 mmol/s and the case where  $NO_2$  and  $I_2$  flow rates are 0.0 mmol/s, and are presented in Figs. 2 – 5. These calculations were premixed. The initial  $O_2(a)$  yield at the exit of the discharge was determined from ElectricOIL  $O_2(a)$  data<sup>11</sup> as a function of rf discharge power; this data had a peak  $O_2(a)$  yield of 12% at 500 Watts of rf power and flow rates of  $O_2:He = 4:16$  mmol/s at the diagnostic port position. As discussed above, the  $O_2(b)$  flow rate was approximately 1.8% of the  $O_2(a)$  flow rate.<sup>34</sup> Data showed that the production of atomic oxygen in the discharge varied linearly with discharge power<sup>11</sup> such that the atomic oxygen flow rate is approximately  $7.5 \times 10^{-4}$  mmol/s per Watt of discharge power for these flow conditions. The total number of Blaze-II simulations performed for this set of simulations was 4800, including the modeling of the individual sections for each run.

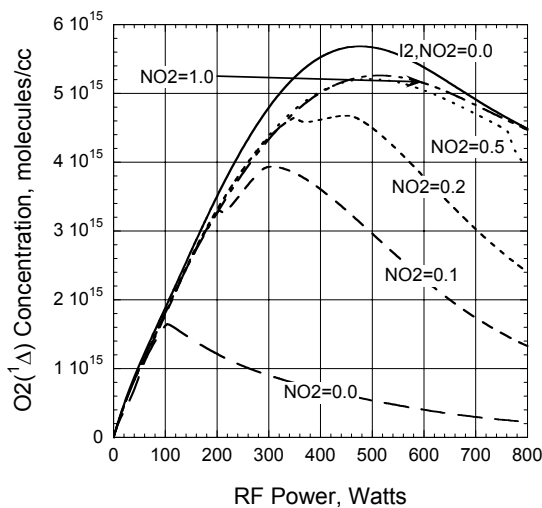


Figure 2: Premixed predictions of  $O_2(^1\Delta)$  concentration at the diagnostic port vs. discharge power vs.  $NO_2$  flow rate.

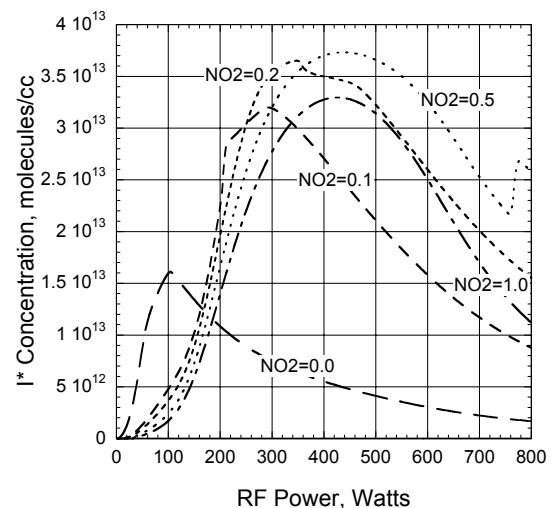


Figure 3: Premixed predictions of  $I^*$  concentration at the diagnostic port vs. discharge power vs.  $NO_2$  flow rate.

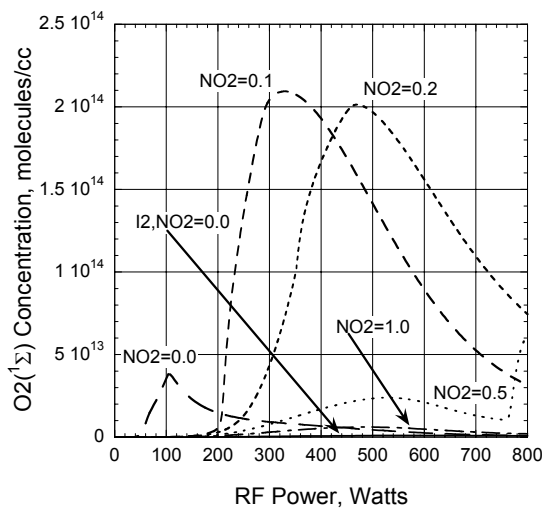


Figure 4: Premixed predictions of  $O_2(^1\Sigma)$  concentration at the diagnostic port vs. discharge power vs.  $NO_2$  flow rate.

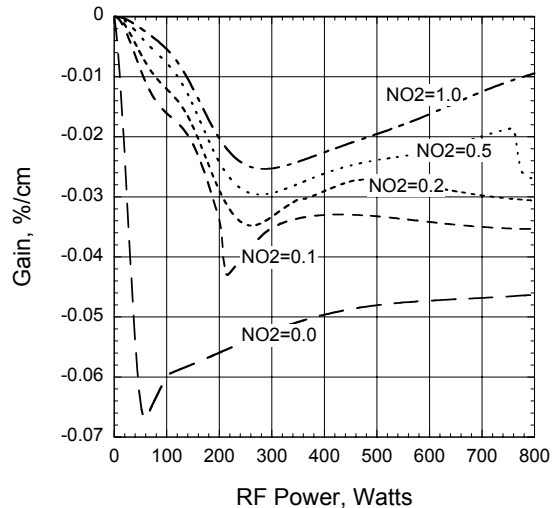


Figure 5: Premixed predictions of gain at diagnostic port vs. discharge power vs.  $NO_2$  flow rate.

The NO<sub>2</sub> flow rates used in ElectricOIL and Blaze-II ElectricOIL calculations are on the order of the O atom flow rate from the discharge. As a result, as discharge power and O atom production are varied as a function of discharge power for a given NO<sub>2</sub> flow rate in the calculations, the equivalence point between the discharge production of atomic oxygen, and titration by NO<sub>2</sub> may be crossed. For the purposes of this study, the O/NO<sub>2</sub> equivalence point is defined for a given NO<sub>2</sub> flow rate as the rf power at which atomic oxygen is produced in the discharge at a rate sufficient to appreciably impact downstream kinetics, despite the removal of atomic oxygen by NO<sub>2</sub> titration and other kinetic processes. In the modeled flow configuration, a quantity of atomic oxygen typically must remain in the flow downstream of the I<sub>2</sub> injection point such that the fast dissociation mechanism of I<sub>2</sub> by atomic oxygen, reactions (78–81), appreciably impacts the downstream kinetics. For example, reactions that are critically dependent upon the presence of atomic oxygen are the fast quenching of I\* by O, reaction (83), and consequently the I\* + O<sub>2</sub>(a) → I + O<sub>2</sub>(b) pooling reaction, reaction (36).

As discharge power is varied, dramatic shifts in the behavior of the model are encountered as these equivalence points are crossed. For the cases plotted in Figs. 2 – 5 with NO<sub>2</sub> flow rates less than or equal to 0.2 mmol/s, the discharge produced flow of O atoms is generally greater than the NO<sub>2</sub> flow rate for most simulated discharge powers. It should be noted however, that a NO<sub>2</sub> flow rate less than the discharge produced atomic oxygen flow rate may still act to completely remove the discharge produced atomic oxygen from the flow by “recycling” of the NO<sub>2</sub> via reactions (84–86) and the subsequent three-body NO recombination reactions (99) and (100). This recycling process is slower than the atomic oxygen removal by full or over-titration with NO<sub>2</sub>. In cases with an NO<sub>2</sub> flow rate of 0.5 mmol/s, the discharge production of O atoms is less than the NO<sub>2</sub> flow rate for discharge powers less than approximately 630 Watts. For cases with an NO<sub>2</sub> flow rate of 1.0 mmol/s, the discharge produced flow of O atoms is less than the NO<sub>2</sub> flow rate for all studied discharge powers. In the premixed calculations, the equivalence points for NO<sub>2</sub> flow rates of 0.1, 0.2, and 0.5 mmol/s occur at rf powers of approximately 300, 450, and 750 Watts of rf power. These points are characterized by a sharp divergence of behavior between concentration and gain curves for the given NO<sub>2</sub> flow rate and the curves for the next largest NO<sub>2</sub> flow rate, Figs. 2 – 5, particularly as seen in O<sub>2</sub>(a) concentration curves, Fig. 2.

For comparative purposes, the corresponding experimental data<sup>11</sup> are illustrated here in Figs. 6 – 9. If we compare Figs. 2 – 5 directly with Figs. 6 – 9, respectively, it becomes clear that there are both many similarities as well as some significant differences:

1. There are strong qualitative similarities in the character of the O<sub>2</sub>(a) curves (Figs. 2 and 6) and I\* curves (Figs. 3 and 7) for NO<sub>2</sub> flow rates of 0.0, 0.1, and 0.2 mmol/s. However, for NO<sub>2</sub> flow rates of 0.5 and 1.0 there are dramatic differences which are likely due to mixing these larger quantities of NO<sub>2</sub> into the flow instantly, thereby increasing their impact on the downstream kinetics.

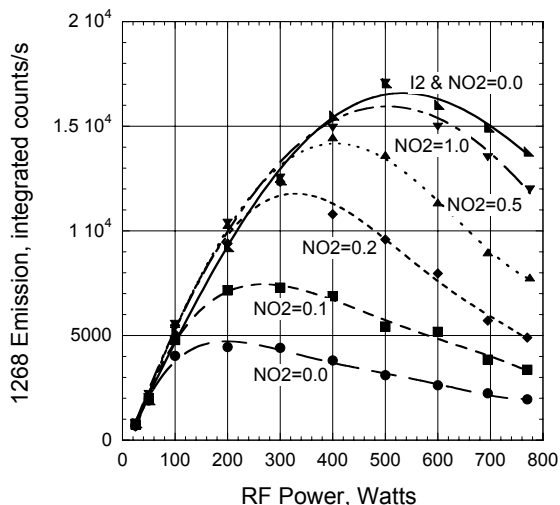


Figure 6: Experimental O<sub>2</sub>(<sup>1</sup>Δ) emission data from ElectricOIL at the subsonic diagnostic port vs. discharge power as a function of NO<sub>2</sub> flow rate.<sup>11</sup>

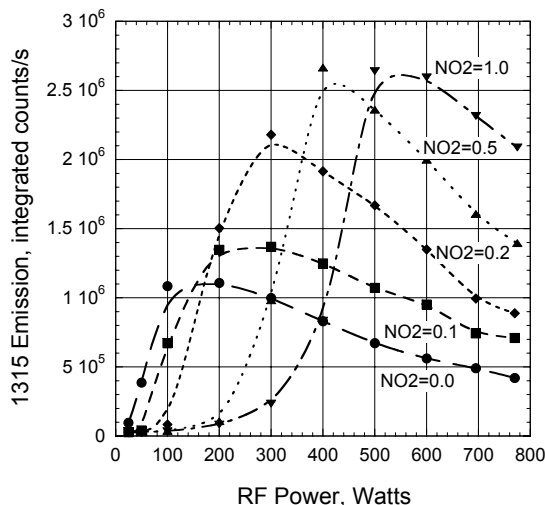


Figure 7: Experimental I\* emission data from ElectricOIL at the subsonic diagnostic port vs. discharge power as a function of NO<sub>2</sub> flow rate.<sup>11</sup>

- There are qualitative similarities between the  $O_2(b)$  (Figs. 4 and 8) and gain curves (Figs. 5 and 9) for  $NO_2$  flow rates of 0.0, 0.1, and 0.2 mmol/s, but again there are dramatic differences for  $NO_2$  flow rates of 0.5 and 1.0 mmol/s which are also likely due to the premixed nature of the calculations.
- Comparing the  $O_2(b)$  curves (Figs. 4 and 8) shows a significant difference for the  $I_2 = 0.0$  mmol/s and  $NO_2 = 0.0$  mmol/s case. In particular the predicted curve is very weak relative to the predictions for the cases with  $I_2$  and with  $NO_2$  or 0.0, 0.1, and 0.2 mmol/s. This suggests that there may be too much  $O_2(b)$  production via  $I$  and  $O_2(a)$  pooling, reaction (36), predicted by the model in the presence of iodine.

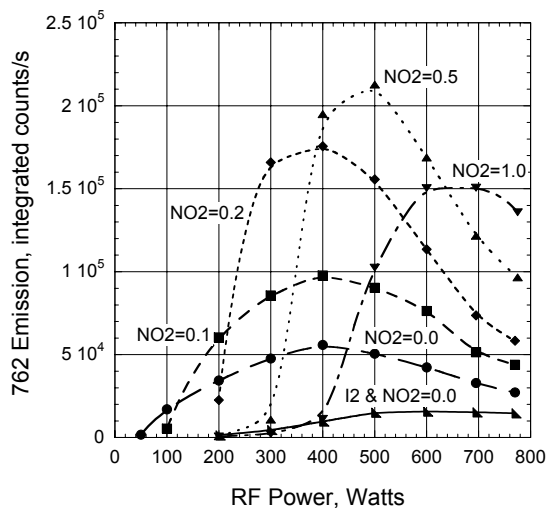


Figure 8: Experimental  $O_2(^1\Sigma)$  emission data from ElectricOIL at the subsonic diagnostic port vs. discharge power as a function of  $NO_2$  flow rate.<sup>11</sup>

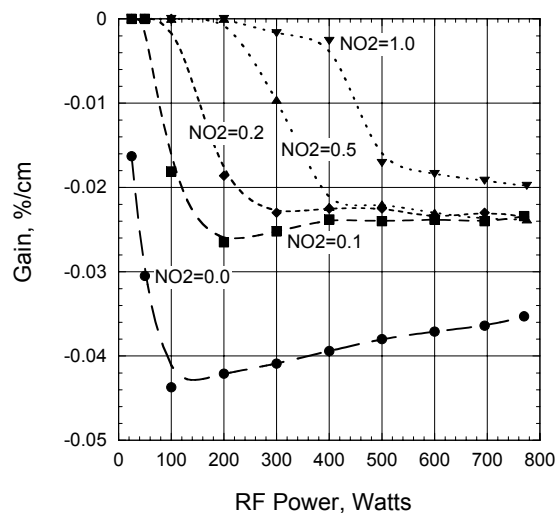


Figure 9: Experimental gain data from ElectricOIL at the subsonic diagnostic port vs. discharge power as a function of  $NO_2$  flow rate.<sup>11</sup>

The most dramatic difference between the calculations and the data is the fact that the model does not predict the correct qualitative behavior for the high  $NO_2$  flow rates of 0.5 and 1.0 mmol/s. Specifically, the  $NO_2 = 0.5$  and 1.0 mmol/s equivalence points are not crossed as they are in the data. The data shown in Figs. 6 – 9 suggest that a significant fraction of the  $I_2$  is being dissociated for the  $NO_2 = 0.5$  mmol/s, rf power  $\geq 300$  W cases, and for  $NO_2 = 1.0$  mmol/s, rf power  $\geq 400$  W cases. Because O atoms are the fastest dissociation mechanism for  $I_2$ , reactions (78–81), and because the character of the 0.5 and 1.0 mmol/s  $NO_2$  calculations do not agree with data, we theorize that the concentration of atomic oxygen is not properly represented in these premixed calculations as a result of some or all of several possible factors:

- All of these simulations were performed as premixed calculations where all injection positions were averaged into the flow discontinuously and the calculation then proceeded downstream as fully mixed. Physically, mixing effects may cause regions of the flow where a larger percentage of atomic oxygen produced in the discharge is allowed to remain unmixed in the downstream flow than in premixed calculations.
- Uncertainties in kinetic rates may affect the downstream concentration of atomic oxygen or other species.
- Experimental diagnostics measuring O atom concentration do not access the entire cross-section of the flow, which may not be fully mixed. There is an estimated 15–20% error associated with the experimental atomic oxygen concentration data, but this error is not sufficient to account for the observed differences at high  $NO_2$  flow rates.

We believe that in a mixing simulation, a more significant quantity of atomic oxygen produced by the discharge may remain in the flow for the requisite distance to interact with the  $I_2$ , thus dissociating the  $I_2$  and influencing other kinetics even when there is a flow of  $NO_2$  larger than the equivalence point. In order to test this theory, the above calculations were repeated with Blaze configured to use a two-stream mixing model. This mixing model includes diffusion coefficients based on the thermodynamic properties of the reactants and a surface stretching enhancement<sup>37,38</sup> that uses a simple analytic calculation of the penetration depths of the reactants which are injected transversely to the mean flow. The diffusion coefficients were manually adjusted to provide the best possible agreement with qualitatively observed

mixing lengths (effectively a scheduled mixing model approach) and the data shown in Figs. 6 – 9. Results using the mixing model are presented in Figures 10 – 13.

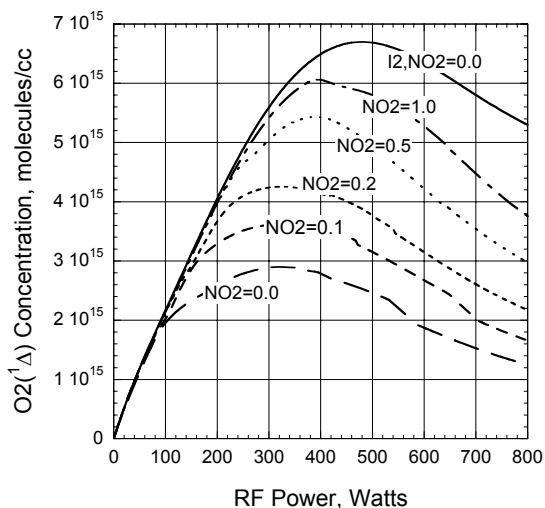


Figure 10: Mixing predictions of  $O_2(^1\Delta)$  concentration at the diagnostic port vs. discharge power vs.  $NO_2$  flow rate.

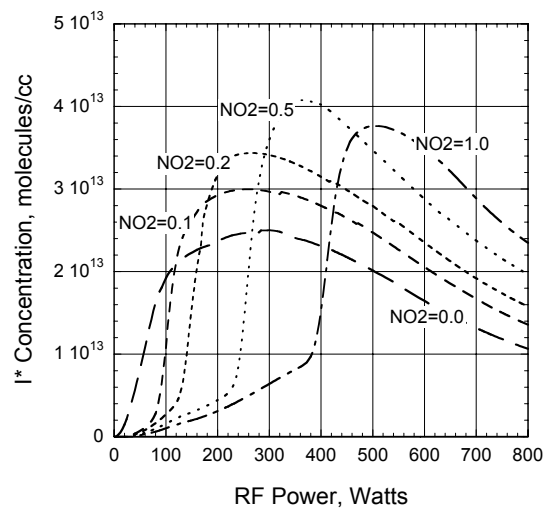


Figure 11: Mixing predictions of  $I^*$  concentration at the diagnostic port vs. discharge power vs.  $NO_2$  flow rate.

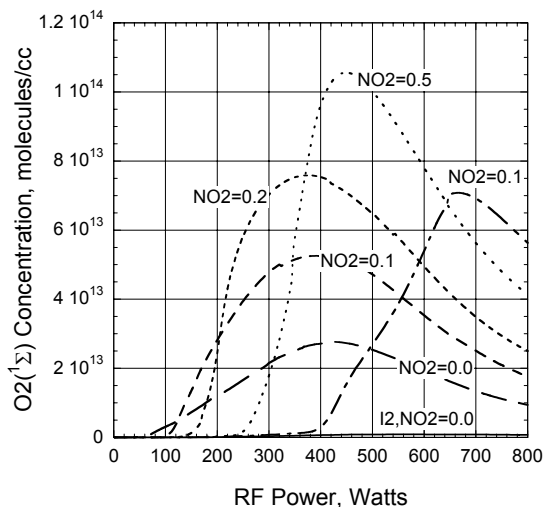


Figure 12: Mixing predictions  $O_2(^1\Sigma)$  concentration at the diagnostic port vs. discharge power vs.  $NO_2$  flow rate.

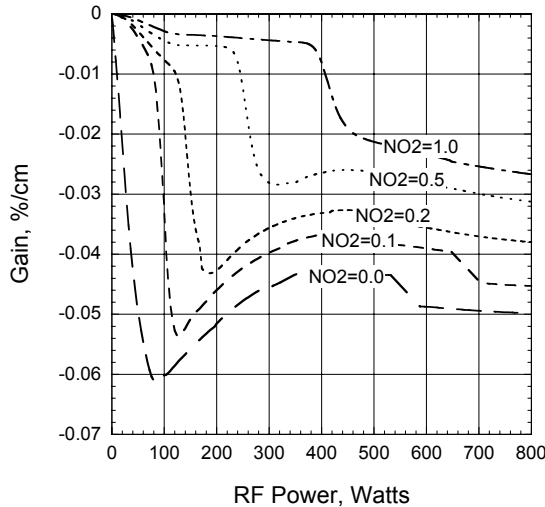


Figure 13: Mixing predictions of gain at the diagnostic port vs. discharge power vs.  $NO_2$  flow rate.

The mixing model predictions for  $O_2(a)$ ,  $I^*$ , and  $O_2(b)$  concentrations and gain, Figs. 10 – 13, are in better agreement with data, Figs. 6 – 9, than premixed model predictions, Figs. 2 – 5. The equivalence points between  $NO_2$  and atomic oxygen occur at the correct rf power levels in the mixing calculations for each  $NO_2$  flow rate. The  $NO_2/O$  equivalence points as a function of rf power were tuned by adjusting the  $NO_2$  mixing rate (note that once the mixing rates for  $NO_2$  and  $I_2$  are tuned for a particular set of flow rates, that the mixing adjustment factor was then held fixed for all other  $NO_2$  and  $I_2$  flow rates). The mixing model predictions for the relative magnitudes of  $I^*$  and  $O_2(b)$  concentration as a function of  $NO_2$  flow rate, Figs. 11 and 12, are in significantly better agreement with data, Figs. 7 and 8, than are the premixed predictions, Figs. 3 and 4. However, the mixing model still appears to over-predict the concentration of  $O_2(b)$  as a function of  $NO_2$  flow rate and rf power with iodine in the flow with respect to the case without iodine and without  $NO_2$  ( $I_2$ ,  $NO_2=0.0$  mmol/s). Since the primary kinetic pathway sustaining  $O_2(b)$  concentration in the flow is  $O_2(a)$  and  $I^*$  pooling to  $O_2(b)$ , reaction (36), and since the uncertainty in the experimental  $I_2$  flow rate is large, either an error in the input  $I_2$  flow rate or the reaction rate  $k_{36}$  (or a combination of both) could explain this error. The mixing model

predictions for the absolute magnitudes of gain as a function of  $\text{NO}_2$  flow rate and rf power, Fig. 13, are also in better agreement with data, Fig. 9, than are the premixed model predictions, Fig. 5. Overall, the mixing model predictions for  $\text{O}_2(\text{a})$ ,  $\text{I}^*$ , and  $\text{O}_2(\text{b})$  concentrations and gain as a function of  $\text{NO}_2$  flow rate and rf power are in very good agreement with data indicating that mixing effects are a critical component of ElectricOIL simulations. Agreement between the Blaze-II model and data may be further improved by continued study of critical kinetics and more accurate determination of input conditions, discharge atomic oxygen yield and  $\text{I}_2$  flow rate in particular.

#### 4. BLAZE-II GAIN AND POWER PREDICTIONS

Blaze-II mixing calculations were performed with the 28 specie, 105 reaction set to model current ElectricOIL gain data as a function of  $\text{I}_2$  flow rate. Cases modeled used reactant flow rates of  $\text{O}_2:\text{He}:\text{NO}$  of 3:16:0.15 mmol/s with  $\text{I}_2$  flow rates of 0.008, 0.014, and 0.036 mmol/s at a total pressure of 12.6 Torr. This set of flow conditions were chosen for gain and power modeling because more precise gain data in the supersonic laser cavity were available for these conditions. Simulations assumed 450 Watts of rf discharge power. The  $\text{O}_2(\text{a})$  yield at the exit of the discharge was determined from ElectricOIL data<sup>14</sup> for  $\text{O}_2:\text{He}:\text{NO} = 3:16:0.15$  mmol/s flow conditions at 450 Watts of rf discharge power. Atomic oxygen yield was estimated at 450 Watts of rf power from  $\text{NO}_2$  titration experiments<sup>34</sup> for the above conditions with  $\text{NO}$  in the discharge and a numerical study. Estimates<sup>34</sup> from titration experiments indicate that the O atom flow rate is  $\sim 0.13$  mmol/s at the  $\text{NO}_2$  injectors. Calculations were performed for various discharge atomic oxygen yields and it was determined that an O flow rate of 0.25 mmol/s at  $X = 0$  cm simultaneously provided reasonable agreement with cavity gain data and O atom flow rate estimates at the  $\text{NO}_2$  injectors. The O atoms decay significantly with flow distance in the presence of  $\text{NO}$  via reactions (99) and (100), Table 1.

All of the simulations discussed in this section used the same mixing parameters determined in Section III. For the flow conditions discussed above with an rf power of 450 W, the predicted  $\text{O}_2(\text{a})$  yield as a function of distance from the discharge exit is shown in Fig. 14 for three different  $\text{I}_2$  flow rates. There are four interesting features that are observed in Fig. 14:

1. the initial drop in  $\text{O}_2(\text{a})$  yield occurring until  $\text{I}_2$  injection is due to the three-body quenching  $\text{O}_2(\text{a})+\text{O}_2+\text{O} \rightarrow \text{O}_2+\text{O}_2+\text{O}$ , reaction (98); the pooling reaction  $\text{O}_2(\text{a})+\text{O}_2(\text{a}) \rightarrow \text{O}_2(\text{b})+\text{O}_2$ , reaction (1); and quenching by O,  $\text{O}_3$ , and  $\text{O}_2(\text{a})$ , reactions (68), (77), and (2) respectively, in order of significance;
2. higher  $\text{I}_2$  flow rates result in lower  $\text{O}_2(\text{a})$  yields downstream in the laser cavity, which is in large part due to the effects of the  $\text{I}^* + \text{O}$  quenching reaction (83) because the atomic oxygen concentration at the  $\text{I}_2$  injection point is still approximately 30% of the discharge exit value;
3. the decrease in yield decay after the cold  $\text{N}_2$  injection occurs in part from the  $\text{O}_2(\text{b}) + \text{N}_2 \rightarrow \text{O}_2(\text{a}) + \text{N}_2$  deactivation channel, reaction (17), where new  $\text{O}_2(\text{b})$  has been created via  $\text{O}_2(\text{a}) + \text{I}^* \rightarrow \text{O}_2(\text{b}) + \text{I}$ , reaction (36), after the iodine injection position. There is also an effect from the temperature dependence of reactions (1) and (17);
4. the yield after the nozzle throat drops as the equilibrium between the pumping reaction (32) and the reverse pumping reaction (33) shifts further in favor of  $\text{I}^*$  as the temperature drops in the supersonic expansion, which subsequently increases the rate of energy loss through the  $\text{I}^* + \text{O}$  energy channel.

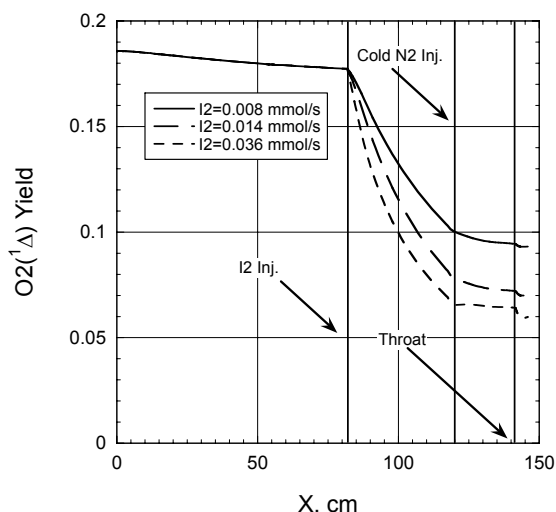


Figure 14: Mixing predictions of  $\text{O}_2(^1\Delta)$  yield as a function of axial position vs.  $\text{I}_2$  flow rate,  $\text{O}_2:\text{He}:\text{NO}:\text{N}_2 = 3:16:0.15:55$  mmol/s.

Figures 15 and 16 illustrate the predicted gain for these three  $\text{I}_2$  flow rates. A large drop in gain (increase in absorption) is observed between the  $\text{I}_2$  injection location and the  $\text{N}_2$  injection location, which is due to the  $\text{I}^* + \text{O}$  quenching that ultimately reduces both the  $\text{I}^*$  and  $\text{O}_2(\text{a})$  concentrations. There is a sudden rise in gain when the cold  $\text{N}_2$  is injected, which is a consequence of the pumping reaction (32) favoring colder temperatures; note that the gain then lowers as

heat is transferred from the warmer wall to the cooler flow between  $N_2$  injection position and the nozzle throat (Blaze-II includes a first order wall heat transfer term). Downstream of the throat the gain increases significantly in the supersonic cavity, Fig. 16. For  $I_2$  flow rates of 0.008, 0.014, and 0.036 mmol/s, the peak gain in the nozzle is predicted to be approximately 0.0085 %/cm, 0.0095 %/cm, and 0.0168 %/cm, respectively. As shown in Fig. 16, the prediction of gain for both the 0.008 mmol/s of  $I_2$  and the 0.036 mmol/s of  $I_2$  cases are in reasonably good agreement with the measured gains<sup>13</sup> of 0.0067 %/cm and 0.0156 %/cm, respectively, for these conditions. (Gain data for the 0.014 mmol/s case was not available).

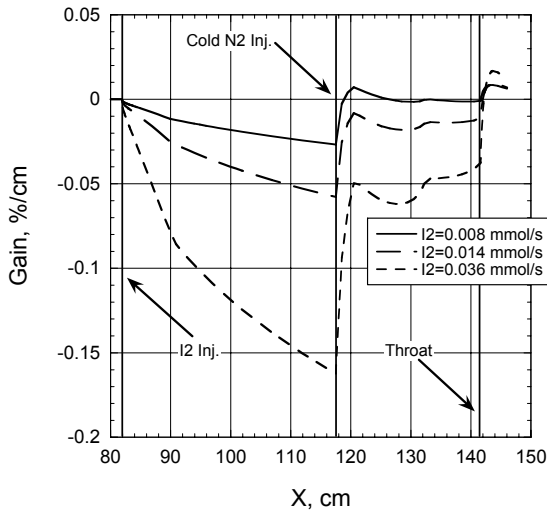


Figure 15: Mixing predictions of gain as a function of axial position vs.  $I_2$  flow rate,  $O_2:He:NO:N_2 = 3:16:0.15:55$  mmol/s.

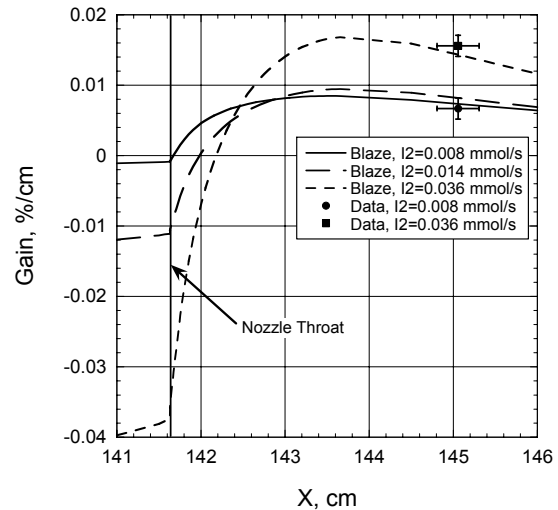


Figure 16: Mixing predictions of cavity gain as a function of axial position vs.  $I_2$  flow rate,  $O_2:He:NO:N_2 = 3:16:0.15:55$  mmol/s.

Power calculations (not shown for brevity) were run for the above gain cases. The predicted powers were a factor of 2 – 4 times larger than the measured powers despite the fact that the gain was well predicted. We believe that this is likely a problem related to the limited dimensionality of the model. The model assumes flow uniformity across the nozzle, and therefore does not account for effects such as a thermal boundary layer that would change the temperature of the nozzle top-to-bottom. The gain, is strongly dependent on temperature, therefore the real device would likely have a gain variation in the vertical direction. The gain data shown in Figs. 15 and 16 were taken along the center of the nozzle flow. If the gain data shown are the peaks of the vertical gain profiles, then the real laser would produce a power output based more on a lower average gain through the laser mode volume. Hence, while Blaze-II is predicting the centerline gain values very well, it is not accounting for higher dimensional effects in the real laser system. Investigation of this with a higher dimensional model along with taking more experimental gain measurements to establish a vertical gain profile is recommended.

## 5. CONCLUDING REMARKS

Recent studies with the ElectricOIL system where the  $O_2(a^1\Delta)$  was produced in a flowing electric discharge, have demonstrated  $O_2(a^1\Delta)$  yields greater than 15%, positive gain, and cw laser power. To better understand the post-discharge physics, premixed and mixing calculations were performed using the generic gas laser model Blaze-II. Blaze-II was adapted to allow the multiple sections/injection-points of reactants used by ElectricOIL, and was enhanced to allow large parametric studies. The Blaze-II kinetics set was significantly updated and now includes 105 reactions and 28 species.

Premixed simulations were run with the updated Blaze-II model and compared with experimental data; many of the trends in the data were modeled reasonably well, but simulations with high  $NO_2$  flow rates were dramatically different. We believe that these simulations did not properly represent the concentration of atomic oxygen in the flow tube principally as a result of using premixed flow simulation rather than mixing simulations. The use of a two stream mixing model provided results that were in significantly better agreement with experimental data for  $I^*$ ,  $O_2(a^1\Delta)$ , and  $O_2(b^1\Sigma)$  concentrations, and gain at the diagnostic port as a function of discharge power and  $NO_2$  flow rate. We believe

that a more accurate understanding of the discharge production of atomic oxygen, kinetic rates, and experimental I<sub>2</sub> flow rates may further improve the accuracy of future Blaze-II calculations in this respect.

Blaze-II was used with the 105 reaction, 28 specie set to model current ElectricOIL gain data as a function of I<sub>2</sub> flow rate. Atomic oxygen yield in the simulated ElectricOIL conditions was estimated to be 0.25 mmol/s at 450 Watts of rf power by baselining the model to NO<sub>2</sub> titration experiment results and gain data. The experimental gain data in the supersonic cavity were modeled well by Blaze-II.

Overall the Blaze-II model with the inclusion of mixing effects appears to be predicting many of the observed qualitative trends that have been measured, and several quantitative comparisons to data are reasonable. However, we believe that improvements can be made to the modeling, especially with the use of higher dimension mixing models. Improvements in the knowledge of the kinetics will likely also play a crucial role in better modeling of the system.

### ACKNOWLEDGEMENTS

This work was supported by the Missile Defense Agency (MDA) through the U.S. Army Space and Missile Defense Command (USA/SMDC) and the Air Force Office of Scientific Research (AFOSR). The authors would like to acknowledge the contributions of: T. Madden and G. Hager (Air Force Research Laboratory); M. Kushner (Iowa St. Univ.); L. Sentman (Univ. of Illinois); T. Rawlins and S. Davis, (PSI, Inc.); M. Heaven and K. Morokuma (Emory University); G. Perram (Air Force Institute of Technology); M. Berman (AFOSR); J. Mulroy (MDA); B. Otey (USA/SMDC); and T. Rakhimova and Yu. Mankelovich (Lomonosov Moscow State University).

### REFERENCES

1. W. McDermott, N. Pchelkin, D. Benard, and R. Bousek, *Appl. Phys. Lett.*, vol. 32, no. 8, pp. 469–470, 1978.
2. D. L. Carroll, J. T. Verdeyen, D. M. King, B. S. Woodard, L. W. Skorski, J. W. Zimmerman, and W. C. Solomon, W. C., *IEEE J. Quant. Elect.*, vol. 39, no. 9, pp 1150–1159, 2003.
3. D. L. Carroll, J. T. Verdeyen, D. M. King, B. S. Woodard, J. W. Zimmerman, L. W. Skorski, and W. C. Solomon, W. C., presented at the AIAA 34th Plasmadynamics and Lasers Conf., Orlando, FL, Jun. 2005, Paper no. 2003–4029.
4. J. Schmiedberger, S. Hirahara, Y. Ichinoche, M. Suzuki, W. Masuda, Y. Kihara, E. Yoshitani, H. and Fujii, *Proc. SPIE*, vol. 4184, pp 32–35, 2001.
5. A. E. Hill, *Proc. Int. Conf. Lasers 2000*, V. Corcoran and T. Corcoran, Eds., McClean, VA, 2001, pp. 249–258.
6. A. A. Ionin, Y. M. Klimachev, A. A. Kotkov, I. V. Kochetov, A. P. Napartovich, L. V. Seleznev, D. V. Sinityn, and G. D. Hager, *J. Phys. D: Appl. Phys.*, vol. 36, pp. 982–989, 2003.
7. T. V. Rakhimova, A. S. Kovalev, K. S. Klopovsky, D. V Lopaev, Yu. A. Mankelevich, A. N. Vasilieva, O. V. Braginsky, N. A. Popov, O. V. Proshina, A. T. and Rakhimov, “Experimental and theoretical study of a pressure scaling possibility of vhf singlet oxygen generator,” AIAA 36th Plasmadynamics and Lasers Conf., Toronto, ON, Jun. 2005, Paper no. 2005–4918.
8. W. T. Rawlins, S. Lee, W. J. Kessler, L. G. Piper, and S. J. Davis, “Advanced diagnostics and kinetics of oxygen-iodine laser systems,” AIAA 36th Plasmadynamics and Lasers Conf., Toronto, ON, Jun. 2005, Paper no. 2005–5299.
9. Yu. V. Kolobyenin, A. A. Adamenkov, Yu. A. Adamenkov, V. V. Bakshin, V. V. Buzoverya, L. A. Vdovkin, B. A. Vyskubenko, L. V. Goryachev, V. I. Efremov, S. P. Ilyin, A. M. Kalashnik, E. A. Kudryashnov, G. S. Rogozhnikov, and Yu. V. Savin, “Gain coefficient in iodine-oxygen laser cavity activated by traveling microwave discharge,” AIAA 36th Plasmadynamics and Lasers Conf., Toronto, ON, Jun. 2005, Paper no. 2005–4920.
10. D. L. Carroll, J. T. Verdeyen, D. M. King, J. W. Zimmerman, J. K. Laystrom, B. S. Woodard, N. Richardson, K. Kittell, and W. C. Solomon, *Appl. Phys. Lett.*, vol. 85, no. 8, pp. 1320–1322, 2004.
11. D. L. Carroll, J. T. Verdeyen, D. M. King, J. W. Zimmerman, J. K. Laystrom, B. S. Woodard, G. F. Benavides, K. Kittell, and W. C. Solomon, *IEEE J. Quant. Elect.*, vol. 41, no. 2, pp. 213–223, 2005.
12. W. T. Rawlins, S. Lee, W. J. Kessler, and S. J. Davis, *Appl. Phys. Lett.*, vol. 86, pp. 051 105–1–3, 2005.
13. D. L. Carroll, J. T. Verdeyen, D. M. King, J. W. Zimmerman, J. K. Laystrom, B. S. Woodard, G. F. Benavides, K. Kittell, D. S. Stafford, M. J. Kushner, and W. C. Solomon, *Appl. Phys. Lett.*, vol. 86, pp. 111 104–1–3, 2005.
14. D. L. Carroll, J. T. Verdeyen, D. M. King, J. W. Zimmerman, J. K. Laystrom, B. S. Woodard, G. F. Benavides, N. R. Richardson, K. W. Kittell, and W. C. Solomon, *IEEE J. Quant. Elect.*, vol. 41, no. 10, pp. 1309–1318, 2005.
15. D. S. Stafford, M. J. and Kushner, *J. of Appl. Phys.*, vol. 96., no. 5, pp. 2451–2465, 2004.

16. L. H. Sentman, M. Subbiah, and S. W. Zelazny, S. "Blaze II: a chemical laser simulation computer program," Bell Aerospace Textron, Buffalo, NY, Tech. Repp. H-CR-77-8, 1977.
17. K. A. Truesdell, S. E. Lamberson, and G. D. Hager, "Phillips laboratory COIL technology overview," AIAA 23th Plasmadynamics and Lasers Conf., Nashville, TN, Jun. 1992, Paper no. 1992-3003.
18. P. G. Crowell, and D. N. Plummer, *Intense Laser Beams and Applications*, SPIE, vol. 1871, pp. 148-180, 1993.
19. P. G. Crowell, "RECOIL: a one-dimensional chemical oxygen iodine laser performance model: part I - theory," RDA Letter No. 87-A/K-3-02-1079, 15 Nov. 1989.
20. D. L. Carroll, *AIAA J.*, vol. 33, no. 8, pp. 1454-1462, 1995.
21. M. C. Heaven, private communication, 2004.
22. J. Han, S. P. Tinney, and M. C. Heaven, *Proc. SPIE*, vol. 5448, pp. 261-268, Sep. 2004
23. A. N. Vasiljeva, K. S. Klopovskiy, A. S. Kovalev, D. V. Lopaev, Y. A. Mankelevich, N. A. Popov, A. T. Rakhimov, and T. V. Rakhimova, *J. Phys. D: Appl. Phys.*, vol. 37, pp. 2455-2468, 2004.
24. R. Atkinson, D. L. Baulch, R. A. Cox, R. F. Hampson Jr., J. A. Kerr, M. J. Rossi, and J. Troe, *J. of Phys and Chem. Ref. Data*, vol. 26, no. 3, pp. 550-962, 1997.
25. I. M. W. Smith, R. P. Tuckett, and C. J. Whitham, Chem. Phys. Lett. No. 0009-2614/92/, vol. 200, no. 6, 1992.
26. G. P. Perram, G. D. and Hager, "The standard chemical oxygen-iodine laser kinetics package," Air Force Weapons Laboratory, Air Force System Command, Kirtland Air Force Base, NM, Final Rep. AFWL-TR-88-50, Oct. 1988.
27. J. Han, A. V. Komissarov, S. P. Tinney, and M. C. Heaven, "Kinetic studies for advanced iodine laser concepts," *Proc. SPIE*, vol. 4971, pp. 45-56, 2003.
28. M. C. Heaven, "Studies of energy transfer processes of relevance to chemically and optically pumped lasers," Air Force Office of Scientific Research, Bolling Air Force Base, Final Rep. AFOSR-TR-95-0012, 1995.
29. M. C. Heaven, Private Communication, 1996.
30. J. J. Deakin, and D. Husain, "Temperature dependence of collisionally induced spin orbit relaxation of electronically excited iodine atoms I( $^2P_5 P_{1/2}$ )," *JCS Faraday Trans. II*, vol. 68, pp. 1603-1612, 1972.
31. G. E. Busch, *IEEE J. Quantum. Electron.*, vol. 17, no. 6, pp. 1128-1133, 1981.
32. J. T. Herron, and D. S. Green, *Plas. Chem. Plasma Process.*, vol. 21, no. 3, pp. 459-481, 2001.
33. F. Kaufman, *Proc. Roy. Soc. A*, vol. 247, pp. 123-139, 1958.
34. J. W. Zimmerman, and D. M. King, Private Communication, 2005.
35. M. C. Heaven, Private Communication, 2005.
36. S. J. Davis, W. J. Kessler, and M. Bachmann, "Collisional broadening of absorption lines in water and atomic iodine relevant to COIL diagnostics," *SPIE*, vol. 3612, pp. 157-166, 1999.
37. R. J. Driscoll, *AIAA J.*, vol. 24, pp. 1120-1126, 1986.
38. R. J. Driscoll, *AIAA J.*, vol. 25, pp. 965-971, 1987.
39. R. Engelman, Jr., B. A. Palmer, S. J. Davis, "Transition probability and collision broadening of the 1.3- $\mu\text{m}$  transition of atomic iodine," *J. Opt. Soc. Am.*, Vol. 73, No. 11, pp. 1585-1589, 1983.